

6 7 **L-Band Dual-Wavelength Fiber Ring Laser with Automated** 8 **Polarization Stabilization and Switching for Remote Sensing** 9 **Applications**

10 S. Tainta^{1,2}, A. Salinas¹, I. Janices¹, U. San-Miguel¹, A. Sanchez-Gonzalez^{1,2}, M. J. Erro^{1,2}, and R. A. Perez-
11 Herrera^{1,2,*}

12 ¹ Department of Electrical, Electronic and Communications Engineering, Public University of Navarra, 31006 Navarra, Spain

13 ² Institute of Smart Cities (ISC), Public University of Navarra, 31006 Navarra, Spain

14
15 **Abstract** – This work reports the experimental demonstration of a dual-wavelength L-band fiber ring laser for remote
16 sensing applications. The system incorporates a polarization-sensitive semiconductor optical amplifier as the gain
17 medium and two fiber Bragg gratings placed 25 km away from the laser cavity using standard single-mode fiber that
18 serve both as wavelength-selective elements and sensing heads. Wavelength switching between single- and dual-
19 channel lasing configurations is enabled by a simplified two-paddle motorized polarization controller. The system
20 achieves optical signal-to-noise ratios exceeding 55 dB and power differences between lasing lines as low as 0.01 dB.
21 To ensure long-term stability, an automatic control algorithm dynamically adjusts the polarization state in real time,
22 compensating for environmentally induced polarization drift. The proposed setup provides a compact and robust
23 solution for polarization-based wavelength switching in fiber lasers, with applications in the field of remote optical
24 sensing.

25 **Keywords:** booster semiconductor optical amplifier, fiber Bragg grating, fiber-optic ring cavity laser, polarization-
26 switchable laser, remote sensing.

27 **1. Introduction**

28 The development of single and multiwavelength fiber-based lasers has been an active area of research for decades, not only
29 as they can serve as optical sources in the C-band of optical fiber communication systems, but also because of their applicability
30 in fields such as sensing or spectroscopy, among others. While mostly developed for the C-band, there have been several
31 proposals also for the L-band (1565-1625 nm), since their use in this wavelength range allows to increase the capacity of fiber
32 links [1], the simplification and improvement of lidar systems [2] and the extension of sensing systems to other contexts [3]. An
33 especially relevant example is the detection of carbon monoxide, carbon dioxide, methane, and other potentially harmful gases
34 with absorption bands in the 1-2 μm spectral region, which has a clear impact in the protection of people and infrastructures
35 in the oil and gas industries, water treatment plants, landfills, and commercial or domestic environments [5]-[7]. One of the most
36 obvious advantages of using optical technologies in this context, the safety they offer by avoiding potentially flammable
37 components, is reinforced if the sensor head can be placed at a distance from the rest of the components, especially if the
38 wavelengths can be remotely switched in order to enable the detection of different gases simultaneously-Switchable L-band
39 multiwavelength lasers have been previously proposed for such applications, primarily based on fiber ring schemes [8]. Erbium
40 doped fiber, which is the usual gain medium at lower wavelengths, presents a reduced emission cross-section beyond 1.6 μm .
41 As a result, achieving sufficient gain at these longer wavelengths requires either longer fiber or higher doping concentrations.
42 Additionally, the strong homogeneous broadening gain that erbium-doped fibers present leads to strong mode competition and
43 results in poor laser stability. Addressing this issue requires the use of more complex setups or additional stabilization techniques
44 [9]-[11]. Semiconductor optical amplifiers (SOAs) are consequently an interesting option as gain media in this wavelength region
45 [12], [13]. In order to enable wavelength selection within the laser cavity, different optical filters are usually included into the
46 ring structure, such as Fiber Bragg Gratings (FBGs) [14], Sagnac filters [8], [15] or Mach-Zehnder interferometers [16], among
47 other techniques. Wavelength switching is typically accomplished by modifying the polarization state within the cavity, altering
48 the ring cavity losses and, consequently, modifying the gain spectral distribution.

49
50 * Corresponding author: rosa.perez@unavarra.es

In [17] authors reported a system for remote sensing applications based on a switchable L-band fiber optic ring cavity laser incorporating a semiconductor optical amplifier (SOA) and multiple FBGs. That study experimentally validated the capability of this architecture to detect temperature variations at remote locations. We demonstrated that by adjusting a motorized fiber polarization controller (PC) located 25 km away from the sensing head the system can be remotely switched between single-wavelength, dual-wavelength, and triple-wavelength lasing configurations. However, since the operation of the setup relies on the polarization properties of the components, the system exhibited limited stability, a common issue in polarization-sensitive architectures [10], [11], [18], [19]. In this work, a simplified version of the configuration described in [17] is presented, reducing the polarization control from three to just two paddles of a motorized PC to remotely achieve the desired wavelength selection. Furthermore, we implement an automatic control mechanism for the PC adjustment, resulting in significantly improved system stability over long periods of time. This approach effectively decouples the sensing information from power fluctuations: while the PC-tuning algorithm compensates for amplitude drifts in the power domain, the sensing data remain encoded in the wavelength shift of the spectral lines, ensuring that the measurement integrity is preserved.

2. Experimental Setup

The experimental configuration of the laser system, depicted in Fig. 1, is based on a fiber-optic laser operating at two distinct wavelengths and implemented using a ring cavity architecture. Notably, the system is implemented using non-polarization-maintaining elements, which represents a worst-case scenario as polarization fluctuations occur throughout the setup. While the use of polarization-maintaining components would likely result in a higher stability and enable a more deterministic output for a given PC configuration, the current setup allows for testing the robustness of the stabilization mechanism. A three-port optical circulator (CIR) is employed to control light propagation within the ring cavity. Optical gain for lasing is provided by an L-band booster-type semiconductor optical amplifier (BOA, model S9FC1080P, from Thorlabs). The circulator directs the amplified signal from the BOA toward a reflective filtering module, enabling the filtered light to be re-coupled into the cavity and ensuring unidirectional propagation of the optical field.

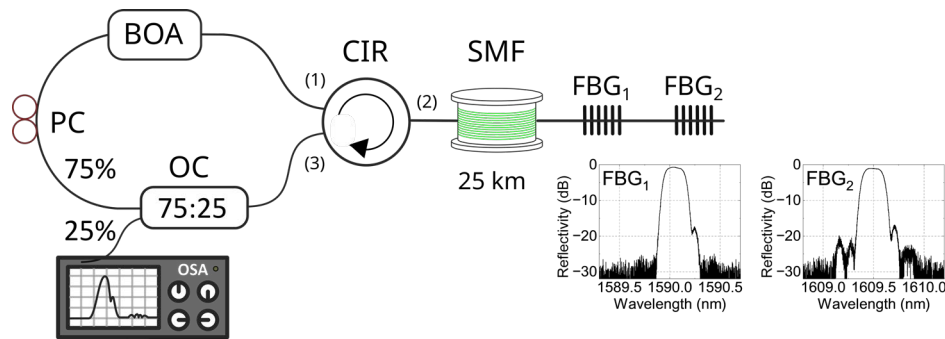
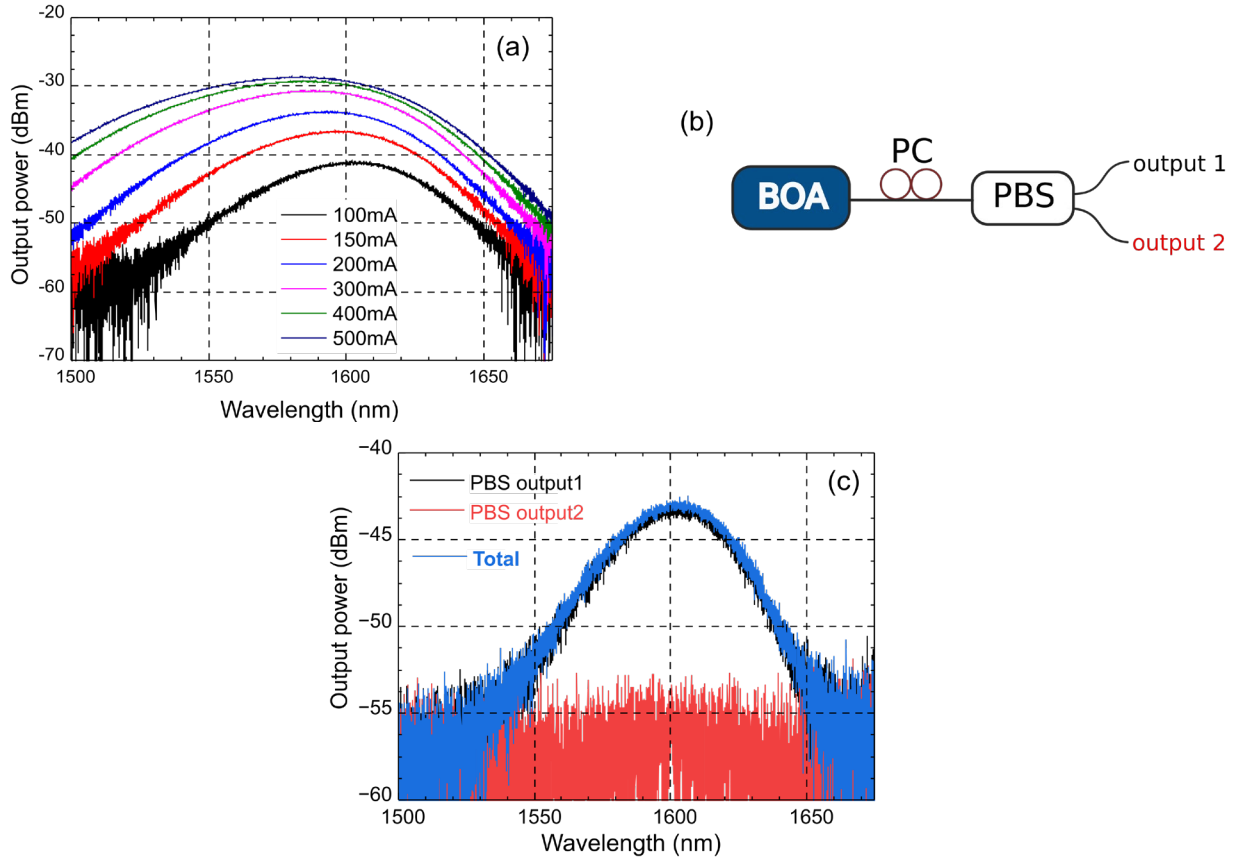


Fig. 1. Experimental setup of the proposed L-band multiwavelength remote sensor based on a motorized polarization-switchable fiber optic ring laser (BOA: Booster Optical Amplifier, PC: Polarization Controller, OC: Optical Coupler, CIR: Circulator, SMF: Single-Mode Fiber, FBG: Fiber Bragg Grating, OSA: Optical Spectrum Analyzer).

Fig. 2 (a) presents the amplified spontaneous emission (ASE) spectra of the BOA at various driving current levels. At a driving current of 500 mA, the BOA exhibits a peak power of -29 dBm at 1583 nm with a 120 nm bandwidth. As observed, increasing the driving current result in both higher output power and a broader emission spectrum while the peak wavelength shifts toward shorter wavelengths. By design the BOA is inherently polarization-sensitive, amplifying only a specific linear polarization state. This property effectively makes the BOA act as a polarization-selective element within the laser cavity. To experimentally demonstrate this behavior, a PC followed by a polarization beam splitter (PBS) were employed to analyze the output polarization dependence as illustrated in Fig. 2 (b). A Thorlabs MTC320 motorized controller was employed to alter polarization via stress-induced birefringence. By coiling single-mode fiber around independent spools to create fractional wave plates, the system, controlled by Thorlabs software, allows for precise polarization adjustment. This PC was used to align the amplification axis of the BOA with one of the PBS outputs. Under these conditions, at a bias current of 100 mA, the BOA

88 delivers a peak output power of -44 dBm at a central wavelength of 1583 nm, consistent with the results shown in Fig. 2 (a).
 89 However, nearly all the power is delivered to the aligned PBS output while the other output port, that corresponds to the
 90 orthogonal linear polarization state, is close to the noise level, as depicted in Fig. 2 (c).



91 **Fig. 2.** (a) ASE spectra at BOA's output for different driving currents; (b) Experimental setup employed for evaluating BOA's
 92 polarization dependence; (c) Output power spectra at the PBS output ports.

93 As shown in Fig. 1, a PC included at the BOA input port allows precise adjustment of the cavity polarization-dependent loss
 94 spectrum and, thus, switching between different wavelength emission configurations. Most lasers that incorporate a PC to ensure
 95 emission at specific wavelengths rely on the fact that only a particular state of polarization (SOP) can resonate within the cavity
 96 [20]-[22]. In conventional three-paddle PCs, formed by a cascade of three retarder plates in the form QWP-HWP-QWP (QWP:
 97 quarter-wave plate, HWP: half-wave plate), precise adjustment of the orientations of the three paddles allows an arbitrary input
 98 polarization to be transformed into a well-defined output SOP [23], thereby enabling resonance at the wavelength associated
 99 with that polarization state. In contrast, in the present work, a reduced two-paddle PC, consisting of a QWP followed by an HWP,
 100 is employed. Although this configuration cannot generate an arbitrary SOP independently of the input, Jones-matrix analysis
 101 shows that it is sufficient to convert a general elliptical polarization into a linearly polarized state with a controllable orientation
 102 by proper adjustment of the plates' angles [24]. When combined with the strong polarization-dependent gain of the BOA, which
 103 is shown in Fig. 2c, this linear polarization rotation translates into distinct cavity gains for different SOPs, enabling
 104 polarization-selective amplification and wavelength switching without the need for a full three-paddle PC. Hence, with only two
 105 paddles to be adjusted instead of the usual three, the tuning process for selecting the desired lasing configuration becomes simpler
 106 and faster. The ring is closed with a 75:25 coupler that extracts part of the generated light for its measurement with an optical
 107 spectrum analyzer with a resolution of 0.03 nm, (OSA, model MS9740B-009, from Anritsu).

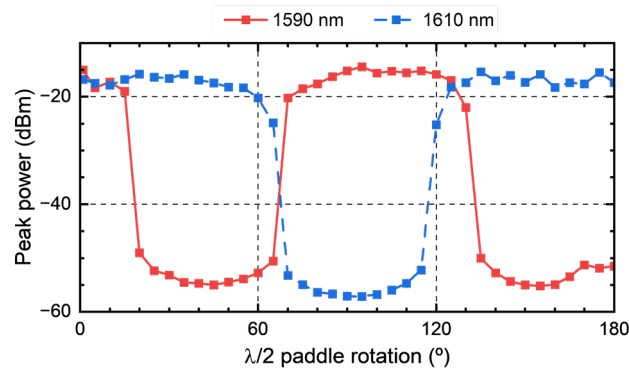
108 The filter used to define the emitted lines wavelengths is constructed by concatenation of two fiber Bragg gratings (FBGs).
 109 Their central wavelengths, 1590 nm (FBG₁) and 1610 nm (FBG₂), are positioned within the BOA's L-band ASE spectrum. As
 110 illustrated in Fig. 1, both FBGs exhibit a 0.22 nm bandwidth with reflectivities of -0.75 dB and -1.05 dB, respectively. Despite

111 a minor mismatch in reflectivities, the variation is insufficient to inhibit dual-wavelength operation. Besides their filtering
112 function, these FBGs are separated from the rest of the setup by a 25 km spool of single mode fiber (SMF), serving also as the
113 remotely controlled sensing mechanism, as demonstrated in [17], and enabling long distance sensing applications. All
114 experimental measurements were conducted at room temperature, and no vibration isolation or temperature compensation
115 techniques were employed.

116 3. Results

117 The switchable operation of the system is validated by driving the BOA at bias currents of 250, 300, and 350 mA, with all
118 measurements performed at room temperature. The laser emission configuration is controlled by adjusting the rotation of both
119 PC paddles. To explore the full range of possible operating modes under different biasing conditions, all configurations -namely
120 no-lasing, single-wavelength, and dual-wavelength states- are systematically tuned using a search algorithm. This algorithm
121 evaluates all possible paddle configurations of the motorized polarization controller (PC) and optimizes different parameters
122 depending on the target configuration. For single-wavelength and no-lasing states, the paddle positions are optimized to
123 maximize suppression of undesired emission lines. For dual-wavelength operation, the optimization minimizes the optical power
124 difference between the two lasing peaks, ensuring balanced output across both channels.

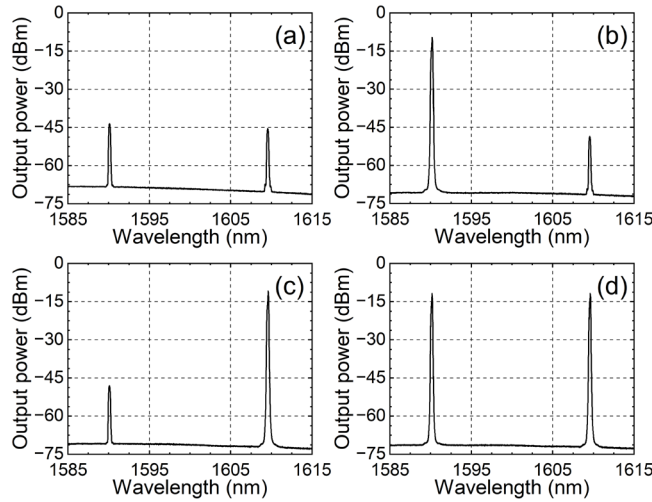
125 An example of the tunability of the system can be seen in Fig. 3. In this example, the QWP is held fixed while the HWP is
126 rotated to different positions with a 5-degree resolution. As shown, different combinations of optical power for the emission
127 wavelengths can be achieved depending on the paddle positions. Therefore, by simultaneously adjusting both paddles, an
128 optimization process can be performed to obtain the desired output combinations.
129



130
131 **Fig. 3.** Optical peak power for each emission wavelength as a function of the HWP adjustment, with the QWP held fixed.

132 The results of the tuning process for all lasing configurations at a bias current of 300 mA are shown in Fig. 4. Fig. 4 (a)
133 corresponds to the no-lasing configuration, where both emission wavelengths exhibit a power level below -45 dBm. In contrast,
134 the single-wavelength emission configurations presented in Fig. 4 (b) and 4 (c) show that both emission lines exceed a peak
135 optical power of -15 dBm, resulting in an optical signal-to-noise ratio (OSNR) greater than 55 dB in both cases, as well as a main
136 lobe-to-sidelobe suppression ratio (MSSR) exceeding 40 dB. Finally, Fig. 4 (d) illustrates the dual-wavelength configuration,
137 where the peak output power of each emission wavelength is -11.84 dBm. The power difference measured in this configuration
138 is less than 0.01 dB, and the OSNR for both wavelengths is higher than 60 dB. These parameters align with established standards
139 for high-performance laser-sensing in the C [25], O [26], and L-bands [3].
140
141

142



143
144

Fig. 4. Output spectra measured in the optical domain for the (a) no-lasing, (b) single-wavelength at 1590 nm (c) single-wavelength at 1610 nm and (d) dual wavelength lasing configurations, for a biasing current of 300 mA at the BOA.

145
146
147
148
149
150
151
152
153
154

Table 1 provides a comprehensive summary of the results obtained for all configurations across the three bias current levels. The data include the power OSNR of each emission line, along with the power difference between both lines for each configuration. The results are consistent across all cases, with only minor variations attributed to increased available power at higher bias currents. In all non-lasing cases, line suppression exceeds 42 dB, while in all single-line emission configurations, the MSSR is at least of 37 dB and the OSNR is greater than 55 dB. For the dual-wavelength emission configuration, the OSNR surpasses 58 dB in all cases, with the maximum power difference between emission lines remaining below 0.5 dB and reaching as low as 0.01 dB in one instance, demonstrating an exceptional level of output equalization. It is worth noting that these results could be further improved with enhanced polarization control, which was limited in this study by the minimum rotation angle of the motorized polarization controller, which was limited to 0.2°. Nonetheless, the results validate the proposed system and demonstrate its ability to maintain high performance under varying operational conditions.

155

Table 1. Switching results for different configurations and biasing currents.

		Peak power (dBm)		OSNR (dB)		Peak power diff. (dB)
		λ_1	λ_2	λ_1	λ_2	$\lambda_1 - \lambda_2$
250 mA	No-lasing	-52.2	-52.4	18.8	18.6	0.2
	λ_1 lasing	-10.1	-51.9	61.8	20.1	41.8
	λ_2 lasing	-48.8	-11.9	23.2	60.0	36.9
	$\lambda_1 + \lambda_2$ lasing	-12.7	-13.1	59.4	58.8	0.5
300 mA	No-lasing	-43.5	-45.6	25.5	23.4	2.0
	λ_1 lasing	-9.7	-48.3	61.0	22.0	38.9
	λ_2 lasing	-48.1	-10.8	22.7	60.0	37.3
	$\lambda_1 + \lambda_2$ lasing	-11.8	-11.8	59.5	59.5	0.0
350 mA	No-lasing	-49.4	-50.0	21.1	20.5	0.6
	λ_1 lasing	-8.3	-50.7	62.2	19.8	42.4
	λ_2 lasing	-54.0	-14.4	16.9	56.6	39.6
	$\lambda_1 + \lambda_2$ lasing	-10.7	-10.8	60.0	60.0	0.1

156

157 The dual-wavelength configuration with a 300 mA bias current was chosen to evaluate the stability of the system. First, output
 158 spectra were captured every 45 seconds for a total of 2.5 hours, without any adjustments of the PC during all the experiment
 159 duration. The registered evolution of the two wavelengths peak powers is plotted in Fig. 5(a), showing that the system is not able
 160 to preserve the dual-wavelength emission, since the 1610 nm line power progressively decreases and eventually falls drastically
 161 after approximately two hours, becoming then the laser a single line device. This behavior prevents the use of this free-operating
 162 setup in optical sensing applications requiring stable long-term dual wavelength operation.

163 Since the cause of the undesired variations of the generated spectrum are the unavoidable random fluctuations of the
 164 polarization state of the light propagating within the ring, an automatic control loop was included to respond and recover from
 165 these oscillations. The operational procedure of the control loop begins with an initialization phase to identify a reference angular
 166 configuration that achieves the desired spectral configuration. Once this configuration is achieved, the system continuously
 167 monitors the optical power spectrum and triggers a local search algorithm if the difference between the peak powers of the
 168 desired spectrum and the measured spectrum exceeds a 1 dB threshold. This search prioritizes the HWP due to its critical impact
 169 on equalization, testing positive and negative angular variations of increasing magnitude until an error below 0.5dB is achieved
 170 again. Should no valid equalization be found by rotating only the HWP, the algorithm selects the best-performing angle and
 171 subsequently adjusts the QWP rotation to identify the optimal combination within the search interval by following a similar
 172 procedure. While this mechanism significantly improves the management of slow drifts, the search process itself introduces
 173 transient fluctuations, such as momentary drops in emission lines, indicating that the current implementation is not yet fully
 174 optimized for all operating conditions. However, as undesired polarization fluctuations typically occur at slower rates than the
 175 time required for the control loop to reoptimize the PC positions, this scheme correctly anticipates and prevents significant
 176 deviations in the produced spectrum, resulting in an important improvement on the stability over long periods of continuous
 177 operation of the laser. When the control loop is enabled, the output spectrum remains stable, as demonstrated in Fig. 5 (b)-(d),
 178 over an extended 5 hours recording period. In Fig. 5 (b) the mean value of the peak powers for both wavelengths is presented,
 179 where the maximum fluctuation of the signal is 1.34 dB for a 95% confidence level (CL). Additionally, Fig. 5 (c-d) show the
 180 peak powers of each wavelength, which present a maximum fluctuation of 2.13 dB and 1.71 dB respectively for a 95% CL.
 181 These fluctuations could potentially be further reduced, since the algorithm currently adjusts the PC paddles only when the power
 182 difference between the two lines exceeds a predefined threshold, without accounting for the individual variation trends.
 183 Additionally, as previously noted, the resolution of the control is constrained by the minimum rotation step of the paddles in our
 184 device, which is 0.2° .

185
 186
 187
 188
 189

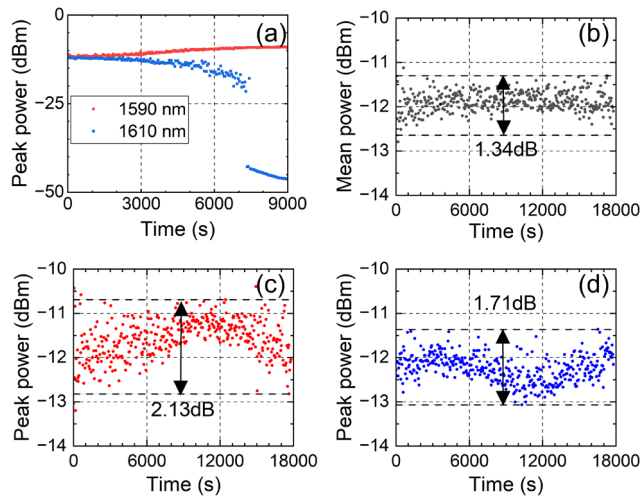


Fig. 5. (a) Output peak powers for a dual-wavelength configuration in free-running mode; (b) mean peak power; (c) 1590 nm and (d) 1610 nm peak for the dual-wavelength configuration with the stabilization loop activated, indicating the CL at 95% (dashed lines).

4. Conclusion

A multiwavelength switchable fiber ring laser operating in the L-band for sensing applications has been experimentally demonstrated. The system is based on a polarization-sensitive SOA as the gain medium and two FBGs that define the emitted wavelengths and that can simultaneously function as remote sensing elements. The FBGs were deployed 25 km from the system header via standard single-mode fiber, thereby enabling long-range remote sensing applications. The laser can be electronically switched at the header between all emission configurations -no lasing, single-wavelength, or dual-wavelength operation-- with optical signal-to-noise ratios (OSNR) consistently exceeding 55 dB, main sidelobe suppression ratios (MSSR) of at least 37 dB, and power differences between lasing lines in the dual-wavelength configuration below 0.5 dB. Wavelength switching is enabled by a simplified motorized polarization controller composed of only two paddles (a QWP followed by a HWP), without the need for additional polarization-dependent elements. This configuration supports automatic control, enabling stable long-term operation without the need for environmental isolation or polarization-maintaining fiber thanks to a closed loop algorithm that self-stabilizes the output by fine-tuning the paddles rotations.

Acknowledgments

Funding

This work was supported in part by projects PID2022-137269OB, funded by MCIN/AEI/10.13039/501100011033 and FEDER “A way to make Europe” and PID2019-104426GB-100 funded by MCIN/AEI, and the Public University of Navarre collaboration grants.

Conflicts of interest

The authors have nothing to disclose.

Data availability statement

The datasets generated and/or analyzed during the current study are not publicly available, but are available from the corresponding author on reasonable request.

Author contribution statement

Conceptualization, S.T., M.J.E. and R.A.P-H.; Methodology, S.T., M.J.E. and R.A.P-H; Software, A.S., A.S-G., S.T., M.J.E. and R.A.P-H; Validation, A.S., I.J., U.S-M, A.S-G.; Formal Analysis, S.T, M.J.E. and R.A.P-H.; Investigation, S.T, M.J.E., A.S-G. and R.A.P-h.; Resources, S.T., M.J.E. and R.A.P-H.; Data Curation, A.S., I.J., U.S-M, A.S-G.; Writing – Original Draft Preparation, S.T, M.J.E. and R.A.P-H.; Writing – Review & Editing, S.T., A.S., I.J., U.S-M, A.S-G., M.J.E. and R.A.P-H.; Visualization, A.S., I.J., U.S-M, A.S-G.; Supervision, S.T., M.J.E. and R.A.P-H.; Project Administration, S.T., M.J.E. and R.A.P-H.; Funding Acquisition, S.T., M.J.E. and R.A.P-H.

References

- [1] Lopez V, Zhu B, Moniz D, Costa N, Pedro J, Xu X, Kumpera A, Dardis L, Rahn J, and Sanders S, Optimized design and challenges for C&L band optical line systems, *J. Lightwave Technol.*, 38, 5 (2020). <https://doi.org/10.1109/JLT.2020.2968225>.

- 225 [2] Wang KX, Gao CQ, Lin ZF, Wang Q, Gao MW, Huang S, and Chen CY, 1645 nm coherent Doppler wind lidar with
226 a single-frequency Er:YAG laser, *Opt. Expr.*, 28, 10 (2020). <https://doi.org/10.1364/OE.392092>.
- 227 [3] Perez RA, Ullan A, Leandro D, Fernandez-Vallejo M, Quintela MA, Loayssa A, Lopez-Higuera JM, and Lopez-Amo
228 M, L-Band multiwavelength single-longitudinal mode fiber laser for sensing applications, *J. of Lightwave Technol.*,
229 30, 8 (2012). <https://doi.org/10.1109/JLT.2011.2174138>.
- 230 [4] Sato H, Saito N, Akagawa K, Wada S, and Tashiro H, Electronically tunable-laser light sources for near infrared
231 spectroscopy, *J. Near Infrared Spectrosc.*, 11, 4 (2003). <https://doi.org/10.1255/jnirs.375>.
- 232 [5] Hu M, Hu M, Wang W, and Wang Q, Wavelength-scanned all-fiber cavity ring-down gas sensing using an L-band
233 active fiber loop, *Appl. Phys. B*, 128, 30 (2022). <https://doi.org/10.1007/s00340-022-07757-3>.
- 234 [6] Zhang H, Bi S, Zhang Q, Tian C, and Wang Z, The fiber ring laser intra-cavity gas sensor for C₂H₂ and CO₂
235 detection based on photoacoustic spectroscopy, *Infrared Phys. & Technol.*, 131, 104623 (2023).
236 <https://doi.org/10.1016/j.infrared.2023.104623>.
- 237 [7] Marshall J, Stewart G, and Whitenett G, Design of a tunable L-band multi-wavelength laser system for application to
238 gas spectroscopy, *Meas. Sci. Technol.*, 17, 5 (2006). <https://doi.org/10.1088/0957-0233/17/5/S15>.
- 239 [8] Zhai Y, Lu B., Meng L, Chen HI, and Bai J, 1.6 μm tunable and switchable single-frequency erbium-doped fiber
240 laser, *Opt. Expr.*, 32, 22 (2024). <https://doi.org/10.1364/OE.540981>.
- 241 [9] Lin Q, Wang Y, Lv C, Zhang H, Gang T, Zhang C, Yang X, Lu B, and Chen H, Conversion of bound states to noise-
242 like pulses in an L-band mode-locked fiber laser, *Opt. Fiber Technol.*, 94, 104291 (2025).
243 <https://doi.org/10.1016/j.yofte.2025.104291>.
- 244 [10] Zhang J, Lv X, Ren W, Zhang L, Fu S, Ren G, Zheng X, Multi-wavelength switchable erbium-doped fiber laser based
245 on single mode- tapered multicore- single mode fiber interferometer, *Opt. Fib. Tech.*, 93, 104215 (2025).
246 <https://doi.org/10.1016/j.yofte.2025.104215>.
- 247 [11] Zhao Q, Pei L, Zheng J, Tang M, Xie Y, and Li J, Switchable, widely tunable and interval-adjustable multi-
248 wavelength Erbium-doped fiber laser based on cascaded filters, *J. of Lightwave Technol.*, 38, 8 (2020).
249 <https://doi.org/10.1109/JLT.2020.2973454>.
- 250 [12] Ummu MA, Madamopoulos N, Joyo A, Kouar M, and Dorsinville R, Tunable multi-wavelength SOA based linear
251 cavity dual-output port fiber laser using Lyot-Sagnac loop mirror, *Opt. Exp*, 19, 4 (2011).
252 <https://doi.org/10.1364/OE.19.003202>.
- 253 [13] Liu T, Jia D, Yang T, Wang Z, and Liu Y, Stable L-band multi-wavelength SOA fiber laser based on polarization
254 rotation, *App. Opt.*, 56, 10 (2017). <https://doi.org/10.1364/AO.56.002787>.
- 255 [14] Yan M, Luo S, Zhang L, Zhang Z, and Xia Y, Triple-wavelength switchable Erbium doped fiber laser with cascaded
256 asymmetric exposure long-period fiber gratings, *Opt. Exp.*, 15, 7 (2007). <https://doi.org/10.1364/OE.15.003685>.
- 257 [15] Sulaiman AH, David AP, Ismail A, Abu Hassan NN, Abdullah F, Jamaludin MZ, and Yusoff NM, Sagnac-
258 interferometer-based multiwavelength SOA fiber laser assisted by an intensity-dependent loss mechanism, *App. Opt.*,
259 63, 5 (2024). <https://doi.org/10.1364/AO.506145>.
- 260 [16] Geng X, Jiang Y, Gu H, Luo S, Sun M, and Li L, Switchable multi-wavelength fiber lasers based on asymmetric
261 biconical fiber tapers, *Opt. Comm.*, 548, 129837 (2023). <https://doi.org/10.1016/j.optcom.2023.129837>.
- 262 [17] Perez-Herrera RA, Janices I, San-Miguel U, Salinas A, Sanchez-Gonzalez A, Erro MJ, and Tainta S, Polarization-
263 switched fiber optic ring laser for L-band multiwavelength remote sensing applications, in *Proc. of 29th International*
264 *Conference on Optical Fiber Sensors, Porto, Portugal, 136397V* (2025), Volume 13639,
265 <https://doi.org/10.1117/12.3062987>.
- 266 [18] Ye G, Liu B, Dai M, Ma Y, Shirahata T, Yamashita S, and Set SY, Pump-power-controlled L-band wavelength-
267 tunable mode-locked fiber laser utilizing nonlinear polarization evolution in all-polarization-maintaining fibers, *Opt.*
268 *Lett.*, 49, 9 (2024). <https://doi.org/10.1364/OL.518882>.
- 269 [19] Aliza HEM, Sulaiman AH, Ismail A, Abdullah F, Yusoff NM, Ibrahim SA, and Jamaludin MZ, Enhanced
270 multiwavelength random fiber laser based on hybrid optical amplifier incorporating Sagnac loop mirror
271 interferometer, *Results in Physics*, 72, 108212 (2025). <https://doi.org/10.1016/j.rinp.2025.108212>.
- 272 [20] Wei L, Xu X, Khatak A, and Henley B, Continuously tunable comb filter based on a high-birefringence fiber loop
273 mirror with a polarization controller, *J. of Lightwave Technol.*, 39, 14 (2021).
274 <https://doi.org/10.1109/JLT.2021.3077252>.
- 275 [21] Feng S, Mao Q, Shan L, and Lit, Reflectivity characteristics of the fiber loop mirror with a polarization controller,
276 *Opt. Comm.*, 277 (2007). <https://doi.org/10.1016/j.optcom.2007.05.016>.
- 277 [22] Hao Y, Miao M, Liao W, and Yang K, Polarization influence on Er³⁺-doped multi-wavelength Brillouin fiber laser
278 based on fiber loop mirror, *Photonics*, 11, 659 (2024). <https://doi.org/10.3390/photonics11070659>.

- 279 [23] Heismann F, Analysis of a reset-free polarization controller for fast automatic polarization stabilization in fiber-optic
280 transmission systems, J. of Lightwave Technol., 12, 4 (1994). <https://doi.org/10.1109/50.285366>
- 281 [24] Heidrich H, Hoffmann D, Helmut CHv, and Ahlers H, Lithium niobate guided-wave network for a coherent receiver,
282 Opt. Lett., 42, 1 (1989). <https://doi.org/10.1364/OL.14.000099>
- 283 [25] S. Pevec and D. Donlagic, "Multiparameter fiber-optic sensors: A review," 464 Opt. Eng., vol. 58, no. 7, Mar. 2019,
284 Art. no. 072009.
- 285 [26] Ahmad, H., Nizamani, B., Melkumov, M. A., & Lobanov, A. S. (2025). Tunable dual-wavelength bismuth-doped
286 fiber laser in O-band using in-line six-mode fiber filter. Optical Fiber Technology, 95, 104393.
287